Jahn-Teller effect in the phonon properties of defective $SrTiO_3$ from first principles

Robert Evarestov,[1] Evgeny Blokhin,[2] Denis Gryaznov,[2,3] Eugene A. Kotomin,[2,3,*] Rotraut Merkle,[2] and Joachim Maier[2]

[1]*Department of Quantum Chemistry, St. Petersburg State University, Peterhof, Russia*

[2]*Max-Planck Institute for Solid State Research, Stuttgart, Germany*

[3]*Institute for Solid State Physics, University of Latvia, Riga, Latvia*

(Received 17 November 2011; revised manuscript received 27 February 2012; published 17 May 2012)

Using a hybrid density functional theory method combined with linear combination of atomic orbitals basis set and periodic supercell approach, the atomic, electronic structure, and phonon properties were calculated for $SrTiO_3$ containing either Fe^{4+} substituting host Ti^{4+} ions or neutral oxygen vacancies V_o. For both defects, the Jahn–Teller effect occurs, thus reducing the cubic symmetry of a perfect crystal and leading to the appearance of both Raman- and infrared-active vibrational modes. The calculated phonon densities of states and group-theoretical analysis of defect-induced phonon frequencies were used for the interpretation of the relevant experimental data, once defect-induced local modes are identified. The temperature dependence of the V_o formation energy based on the calculated Gibbs free energy was also compared with experiments, and the phonon contribution therein estimated.

DOI: 10.1103/PhysRevB.85.174303 PACS number(s): 63.20.dk, 71.20.−b, 31.15.V−, 77.84.Bw

Strontium titanate ($SrTiO_3$) is one of the most prominent functional materials with numerous applications; it serves as a most studied prototype for a wide class of ABO_3-type perovskites.[1,2] The oxygen vacancy V_o is a common defect in perovskites, controlling mass transport properties (e.g. in permeation membranes and solid oxide fuel cell cathodes[3–5]), whereas the Fe impurity substituting for a host B-cation is important for electro- and magneto-optical applications.[6] We are familiar with more than 20 papers dealing with first-principles calculations of the atomic and electronic structure for V_o-only in $SrTiO_3$ (Ref. 7 and references therein). However, the common problem of these calculations is use of the GGA exchange-correlation functionals, which strongly underestimate the band gap of $SrTiO_3$ with the result that the energy level of the vacancy (which is a shallow donor) falls into the conduction band instead of lying in the band gap. On the other hand, the DFT + U functional suggested several scenarios for the position of the defect level, depending on the Hubbard-U parameter.[8,9] A few calculations only used the hybrid exchange-correlation functionals for point defect calculations in perovskites.[7,9–12] These functionals yield accurate description of the structural, electronic, and phonon properties of the perfect $SrTiO_3$ (Ref. 13) and other perovskites.[14,15] In this paper, we calculate the defect-induced phonon spectrum, which is necessary for the interpretation of Raman experiments[16,17] for both types of defects and the prediction of the temperature dependence of the defect formation energy.

Despite the fact that $Sr(Fe_xTi_{1-x})O_3$ solid solutions are relatively well studied both experimentally (e.g. Refs. 17–20) and computationally,[21,22] only two experimental studies have dealt with the vibrational Raman spectra of these systems,[17,20] whereas phonon calculations are practically absent so far (except for a preliminary study[16]). Note also that the Raman-active modes are observed only at the relatively low concentrations of Fe^{4+} Jahn–Teller (JT) defects in $SrTiO_3$, but not for the other end of the solid solution series—$SrFeO_3$ where Fe $3d$ states are delocalized and form broad electronic bands.[22] Moreover, no Raman effect is observed also for oxygen vacancies compensated by Sc^{3+} and Fe^{3+} in $SrTiO_3$ (Ref. 17)—unlike V_o defects compensated by electrons in a reduced crystal—thus indicating that the JT effect (arising due to electronically degenerate Ti^{3+} ions neighboring oxygen vacancies) is a key issue here. The relation between JT effects and Raman-active spectra is the main focus of this paper.

In the present spin-polarized calculations, we use a basis set (BS) of linear combination of atomic orbitals (LCAO) and hybrid exchange-correlation Perdew-Burke-Ernzerhof (PBE0) functional[23] as implemented in the CRYSTAL09 computer code[24] (more details are given in our previous paper[13]). The BS for Fe, Sr, Ti, and O atoms were taken from Refs. 13 and 25 and additionally optimized here for the $Sr(Fe_{0.5}Ti_{0.5})O_3$ solid solution, giving a total energy gain of ∼0.2 eV per supercell. Three different concentrations of the iron impurity were modeled (12.5%, 6.25%, and 3.125%) with full structure optimization using a ($2 \times 2 \times 2$ extended) 40-atom supercell as well as larger, 80- and 160-atom supercells (see Ref. 7 for details). The phonon frequencies were calculated for an iron content of 6.25%, which is a reasonable choice for a proper comparison with the experiment.[17]

The Mulliken atomic charges indicate a considerable covalency of the Ti-O bonding [2.33 e (Ti), −1.46 e (O), 1.95 e (Sr)]. The calculated Fe charge (2.2 e) indicated also a considerable Fe-O bond covalency and is close to the Ti charge. The Fe magnetic moment 3.6 μ_B is close to that expected for a pure ionic model (4 μ_B).

As known,[21] the Fe^{4+} substituting host Ti^{4+} ions in $SrTiO_3$ exhibits the high-spin d^4 state with $S = 2$, i.e. the e_g energy level is occupied by one α electron, whereas the other three α electrons occupy t_{2g} states. This results in the JT $E \otimes e$ effect and asymmetric relaxation of six nearest oxygen atoms surrounding the iron impurity. The geometry optimization in our calculations resulted in the reduction of the Fe-site symmetry from O_h down to the tetragonal symmetry D_{4h}.

In agreement with previous calculations of the JT distortion,[21] four (planar) O atoms were displaced by 0.08 Å inwards, whereas two (axial) O atoms by 0.11 Å outwards Fe ion (given for 3.125% Fe, the changes between 6.25% and 12.5% Fe are insignificant). The lattice energy gain due to the JT optimization is quite considerable, 0.39 eV per supercell. An increase of the iron concentration leads to a decrease of

atomic displacements in agreement with previous theoretical[21] and experimental[17] findings. The dispersion of the Fe-impurity band (within $SrTiO_3$ band gap) strongly decreases, from 1.6 eV for 12.5% to 0.16 eV for 6.25% and 0.1 eV for 3.125% of Fe content. Thus, one can conclude that the Fe concentrations not exceeding 6.25% are necessary to model single Fe^{4+} defects in $SrTiO_3$. Despite the small additional total energy gain (<0.03 eV per supercell) resulting from the tetragonal lattice distortion, the difference in tetragonal lattice parameters c and $a = b$ reaches 0.07 Å, with the trend to decrease for a very small (3.125%) iron content.

For defect-free cubic $SrTiO_3$, no first-order Raman-active vibrational frequencies are allowed according to the selection rules. Such frequencies arise, however, when crystal symmetry is reduced, e.g. due to the phase transition at 105 K[13] or upon formation of point defects (including Fe doping or V_o creation by sample reduction). The phonon frequencies were calculated at the BZ center of a defective supercell within the harmonic approximation.[26] According to the tetragonal symmetry D_{4h}^{17} characteristic for a Fe-containing supercell, three types of phonon modes are allowed: Raman-active (e_g, a_{1g}, b_{1g}, and b_{2g} type), infrared (IR)-active (e_u and a_{2u}) and silent (a_{1u}, a_{2g}, b_{1u}, and b_{2u}) modes. [Two acoustic modes (e_u and a_{2u} type) with frequencies close to zero were also obtained in our study.] The phonon frequencies were smeared according to a normal distribution (smearing width 10 cm^{-1}), in order to obtain the total and atom-projected phonon densities of states (DOS), which are plotted in Fig. 1 for 80-atom supercells. It should be noted that the calculated DOS here represent a semiquantitative picture, as only the Γ point frequencies could be used. The DOS calculated for a perfect crystal [Fig. 1(I)] is generally in good agreement with the experimentally extracted DOS.[27] Detailed analysis of phonons in a pure (cubic and tetragonal) $SrTiO_3$ was presented in Ref. 13, where advantage of hybrid functionals is also demonstrated.

The inclusion of the Fe^{4+} impurity into the otherwise perfect crystal does not change the DOS considerably. Both the experimental spectra[17] and the calculated IR frequencies for Fe^{4+}-doped $SrTiO_3$ are close to those in a perfect crystal. In Fig. 1(II) (atom-projected DOS), one can see the formation of three groups of defect-related modes centered around 150, 300, and 500 cm^{-1}. The phonons involving iron atom movements are always of e_u or a_{2u} type. Indeed, the double degenerate e-type vibrations correspond to the mutually perpendicular Fe movements in a plane of four planar O atoms, whereas a type are out-of-plane Fe motions in the directions of two axial oxygen atoms surrounding an impurity.

Based on the above-mentioned selection rules, we suggest a possible assignment of the experimentally observed Raman frequencies (Table I). The highest frequency (690 cm^{-1}) is due to a localized O stretching vibration mode without Ti and Fe ion motions, whereas the other modes arise due to different types of (Ti, Fe)-O vibrations. Notice that our present calculations on Fe^{4+} in $SrTiO_3$ give practically the same total energy and phonon frequencies as our previous study assuming the point symmetry group C_{4v}.[28]

In the calculations of oxygen vacancies (V_o; site symmetry D_{4h}), we deal with a neutral supercell. However, the electron density of two electrons (remaining from the missing O atom) is redistributed to minimize the total energy of a system.

TABLE I. Comparison of calculated and experimentally observed transverse optical Raman phonon frequencies (cm^{-1}) for $SrTiO_3$ doped with Fe^{4+} ions (SG 139, D_{4h}^{17}).

Experiment (Ref. 17) 10% iron	Modeling 6.25% iron
170	162 (b_{1g}), 178 (a_{1g})
250	239 (b_{2g})
475	475 (b_{2g})
545	547 (a_{1g})
690	752 (a_{1g})

We kept the basis functions from the missing oxygen in the vacancy (so-called ghost atom basis), which considerably improves the agreement of calculated defect formation energy with the experiment (see below). According to the experimental data extrapolated to 0 K,[29] the V_o formation enthalpy (with respect to an O atom in a free O_2 molecule) is ~6.1 eV. Its energy level ($V_o/V_o^{\bullet}$ redox level) lies very close (<0.1 eV) to the conduction band bottom whereas the $V_o^{\bullet\bullet}/V_o^{\bullet}$ redox level lies deeper, i.e. ~0.3 eV.[29] Our vacancy calculations suggest the supercell symmetry D_{2h} with the effective charge of the vacancy close to $V_o^{\bullet}$ and the triplet magnetic state lower in energy than singlet (~0.2 eV per supercell), in agreement with a recent study.[9] The calculated defect energy level at the Γ point of the Brillouin zone (BZ) lies ~0.4 eV below the conduction band but overlaps with it at the other points of the

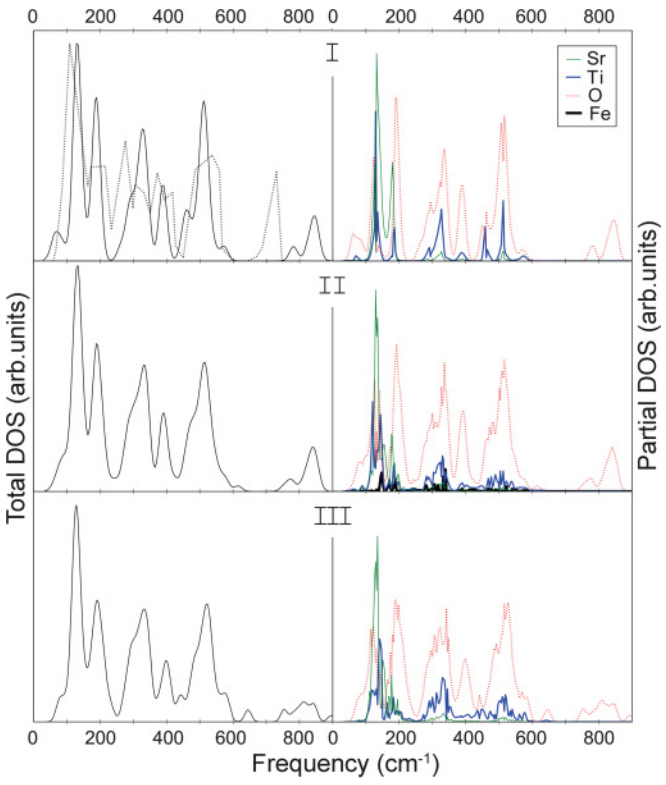

FIG. 1. (Color) The calculated total (left column) and atom-projected (right column) phonon DOS for (I) perfect $SrTiO_3$ [the dotted line is an experimentally extracted total DOS (Ref. 27)], (II) Fe^{4+} doped $SrTiO_3$, and (III) $SrTiO_{3-\delta}$ containing oxygen vacancies. The concentration of both Fe^{4+} and V_o defects is 6.25%. Fe contribution in partial densities is multiplied by a factor of 5.

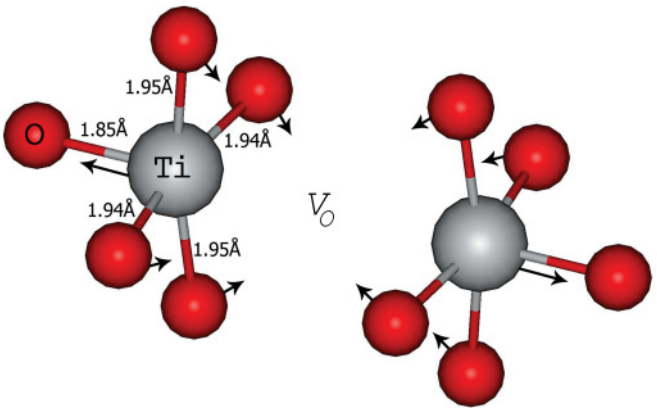

FIG. 2. (Color online) The equilibrium atomic structure with the JT distortion around Ti^{3+} ions near the oxygen vacancy.

BZ. The additional energy reduction responsible for the lifting of double degeneracy of the last occupied energy level (the JT effect) is 70 meV per supercell for 12.5% V_o (symmetry lowers from D^1_{4h} to D^1_{2h}) and 30 meV per supercell for 6.25% V_o (supercell symmetry lowers from D^{17}_{4h} to D^{23}_{2h}). Note that the JT effect was experimentally observed for Ti^{3+} ions after photoexcitation of a pure crystal.[30]

As a result, the charge and spin density of electrons remaining from a removed O atom are quite delocalized in the vicinity of the defect. Two Ti ions are strongly displaced outwards the V_o by 0.11 Å along the (100) axis in the direction of two (axial) O ions which move slightly towards them. Four (planar) O ions in the plane perpendicular to the Ti-V_o axis are divided into two nonequivalent pairs and displaced slightly towards the V_o (Fig. 2). This results in a local lattice distortion which manifests the JT effect. It is interesting to note that the distortion pattern here (axial Ti-O bond shortened relative to planar Ti-O, as expected from a simple ligand-field model for the case of one electron in otherwise degenerate t_{2g} orbitals) is opposite to the Fe^{4+} case (axial bonds elongated, decisive JT contribution arising from the single electron in the e_g orbitals). With the decrease of the defect concentration from 12.5% to 6.25%, the dispersion of the defect band throughout the BZ decreases drastically (from ∼1.0 eV down to 0.2 eV), although the displacement pattern and the charge redistribution around the V_o do not change considerably.

Analyzing the calculated phonon eigenvectors, one can suggest an assignment of the observed Raman spectra [Table II and Fig. 1(III)]. In agreement with Ref. 16, the mode with frequency 135 cm^{-1} is not related to the vacancy but to Sr ion motion. The frequencies of 505 and 630 cm^{-1} correspond to the relative motion of Ti and O ions near the vacancy, whereas the highest frequency around 700 cm^{-1} mainly refers to Ti-O stretching vibrations near the vacancy.

Lastly, we have calculated the standard free energy of oxygen vacancy formation ΔG^0_F as a function of temperature at constant pressure:

$$\Delta G^0_F(T) = \left[E^{V_o}_{\rm tot} + \frac{1}{n}\left(E^{V_o}_{\rm vib} - TS^{V_o}_{\rm vib}\right) + pV^{V_o}\right] - \left[E^{p}_{\rm tot} + \frac{1}{m}\left(E^{p}_{\rm vib} - TS^{p}_{\rm vib}\right) + pV^{p}\right] + \frac{1}{2}\mu^0_{o_2}(T), \quad (1)$$

TABLE II. Comparison of calculated and experimentally observed transverse optical Raman phonon frequencies (cm^{-1}) for reduced $SrTiO_3$ (SG 69, D^{23}_{2h}). Frequencies marked by tildes (∼) were estimated from the experimental spectrum, those marked by asterisks (∗) were observed in defect-free tetragonal $SrTiO_3$ below 105 K.

Experiment (Ref. 16)	Modeling 6.25% V_o
∼135	135 (a_g)
144*	146 (b_{2g})
∼175	174 (b_{2g})
445*	446 (b_{3g})
505	505 (b_{2g})
∼555*	561 (a_g)
630	643 (a_g)
700	753 (a_g)

where superscript p and V_o indicate perfect and defective (one V_o per supercell) crystals, $E^{V_o/p}_{\rm tot}$ total electron energies, $E^{V_o/p}_{\rm vib}$ the vibration contribution to internal energy including vibrations at $T = 0$ K, $S^{V_o/p}_{\rm vib}$ the entropy of vibrations, $V^{V_o/p}$ the supercell volume, T the temperature, and p the standard pressure. All the energies are given per supercell. The prefactors $1/n$ and $1/m$ in Eq. (1) are ratios of the number of atoms in a primitive unit cell to that in the supercell for the defective (one V_o per supercell) and perfect $SrTiO_3$, respectively. For the calculation of the standard chemical potential of O_2 $\mu^0_{O_2}(T)$, we used the free energy of a gas-phase O_2 molecule calculated using the LCAO method within an ideal gas model.[31] This also requires the knowledge of the vibrational properties of O_2. In our calculations on O_2, the rotational and vibrational characteristic temperatures were obtained as 2.11 and 2478.60 K (experiment 2.07 and 2230.0 K[31]), respectively. Note that the LCAO method and the PBE0 functional allow us to reproduce very accurately not

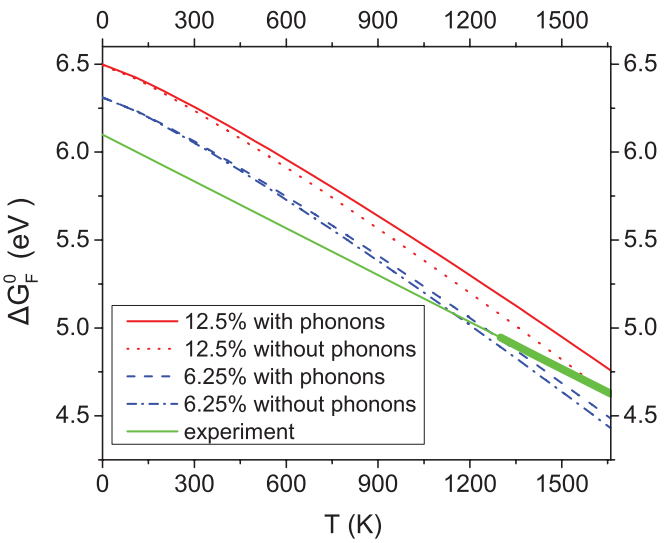

FIG. 3. (Color) The calculated Gibbs formation energy of oxygen vacancy ΔG^0_F as a function of temperature and its comparison to the experiment (Ref. 29). Bold part of the experimental line corresponds to the temperature range of the actual experiments, whereas the rest of the line is an extrapolation to low temperatures.

only the binding energy of a free O_2 molecule (5.30 eV vs experimental 5.12 eV) but also its equilibrium bond length (1.20 Å vs experimental 1.21 Å). Such high-accuracy LCAO calculations make no use of any experimental data for defect formation energies. The standard expressions for $E_{\mathrm{vib}}^{V_o/\mathrm{p}}$ and $S_{\mathrm{vib}}^{V_o/\mathrm{p}}$ within the harmonic approximation are discussed in many reviews (e.g. Refs. 32 and 33).

The calculated ΔG_F^0 and its temperature dependence is presented in Fig. 3 with and without taking into account the phonon contribution in the crystalline phase (which is typically neglected in the literature). The agreement of the calculations for 6.25% of oxygen vacancies with experiments is very good. A larger defect concentration of 12.5% (usually used in the literature) overestimates the defect formation energy at 0 K by ∼0.2 eV. The agreement of theory and experiment at high temperatures is good. Neglecting the ghost basis functions would lead to an additional overestimate of ∼0.5 eV. As expected, the phonon contribution is more significant (∼0.1 eV) at higher temperatures. When comparing theory and experiments, one has to keep in mind that the experimental data (point defect concentrations from which mass action constants are extracted[29]) were determined at high temperatures (1300–1700 K), thus small deviations in the measured temperature dependence may affect the reliability of the extrapolated experimental data at low temperatures.

Summing up, we have shown how the Jahn–Teller-type lattice distortion around two quite different types of defects, Fe^{4+} and V_o, results in Raman- and IR-active phonons. Characteristic defect-induced vibrational modes were deduced from a group-theoretical analysis of results of the first-principles calculations and used for the interpretation of available experimental data. Such an analysis is of prime importance since (i) in contrast to intuition, defect-induced Raman frequencies do not necessarily coincide with those in the phonon spectrum of a perfect crystal, (ii) they do not always involve the motion of the impurity, and (iii) new local Ti-O or Fe-O vibrational modes (absent in the perfect crystal) could or could not be Raman active, depending on the selection rules. The conclusion could be drawn, in particular, that the Raman frequency experimentally observed around 700 cm^{-1} for both defects arises due to a local O ion stretching vibration near the JT defect. The V_o Gibbs formation energy calculated for 6.25% oxygen vacancies taking into account the phonon contribution is in good agreement with the experiment and drops considerably (by ∼0.8 eV) as temperature increases from 300 to 1000 K. The phonon contribution to the V_o formation energy increases with temperature, being ∼5% at 1000 K. The method developed in this paper could be used for a wide class of defects in nonmetallic solids.

This study was partly supported by EC FP7 NASA-OTM Project (Grant Agreement No. 228701) and by a grant of computer time at the EMS Laboratory at PNNL (Project No. 42498). The part of the high performance calculations was performed at the Computer Center of St. Petersburg State University. The authors are grateful to Manuel Cardona, Mike Finnis, and Eugene Heifets for numerous stimulating discussions.

*Corresponding author: kotomin@latnet.lv

[1] M. E. Lines and A. M. Glass, *Principles and Applications of Ferroelectrics and Related Materials* (Oxford University Press, New York, 1977).
[2] J. B. Goodenough, Rep. Prog. Phys. **67**, 1915 (2004).
[3] R. Merkle and J. Maier, J. Angew. Chem. Int. Ed. **47**, 3874 (2008).
[4] J. Sunarso, S. Baumann, J. M. Serra, W. A. Meulenberg, S. Liu, Y. S. Lin, and J. C. Diniz da Costa, J. Memb. Sci. **320**, 13 (2008).
[5] J. Richter, P. Holtappels, T. Graule, T. Nakamura, and L. J. Gauckler, Monatsh. Chem. **140**, 985 (2009).
[6] H. J. Donnerberg, *Atomic Simulations of Electro-Optical and Magneto-Optical Materials*, Vol. 151, Springer Tracts in Modern Phys. (Springer, Berlin, 1999).
[7] Yu. F. Zhukovskii, E. A. Kotomin, R. A. Evarestov, and D. E. Ellis, Int. J. Quant. Chem. **107**, 2956 (2007).
[8] D. Cuong, B. Lee, K. Choi, H. Ahn, S. Han, and J. Lee, Phys. Rev. Lett. **98**, 115503 (2007).
[9] Z. Hou and K. Terakura, J. Phys. Soc. Japan **79**, 114704 (2010).
[10] V. E. Alexandrov, E. A. Kotomin, J. Maier, and R. A. Evarestov, Eur. Phys. J. B **72**, 53 (2009).
[11] Yu. Zhukovskii, E. A. Kotomin, and D. E. Ellis, Solid State Commun. **149**, 1359 (2009).
[12] M. Choi, F. Oba, and I. Tanaka, Phys. Rev. B **83**, 214107 (2011).
[13] R. A. Evarestov, E. Blokhin, D. Gryaznov, E. A. Kotomin, and J. Maier, Phys Rev. B **83** 134108 (2011).
[14] R. A. Evarestov, Phys. Rev. B **83**, 014105 (2011).
[15] D. Gryaznov, R. A. Evarestov, and J. Maier, Phys. Rev. B **82**, 224301 (2010).
[16] D. A. Tenne, I. E. Gonenli, A. Soukiassian, D. G. Schlom, S. M. Nakhmanson, K. M. Rabe, and X. Xi, Phys. Rev. B **76**, 024303 (2007).
[17] M. Vračar, A. Kuzmin, R. Merkle, J. Purans, E. A. Kotomin, J. Maier, and O. Mathon, Phys. Rev. B **76**, 174107 (2007).
[18] R. Waser, J. Am. Ceram. Soc. **74**, 1934 (1991).
[19] I. Denk, W. Münch, and J. Maier, J. Am. Ceram. Soc. **78**, 3265 (1995).
[20] N. van Minh and D. T. T. Phuong, J. Sol-Gel Sci. Technol. **55**, 255 (2010).
[21] R. A. Evarestov, S. Piskunov, E. A. Kotomin, and G. Borstel, Phys. Rev. B **67**, 064101 (2003).
[22] V. Alexandrov, J. Maier, and R. A. Evarestov, Phys. Rev. B **77**, 075111 (2008).
[23] J. P. Perdew, M. Ernzerhof, and K. Burke, J. Chem. Phys. **105**, 9982 (1996).
[24] R. Dovesi, V. R. Saunders, C. Roetti, R. Orlando, C. M. Zicovich-Wilson, F. Pascale, B. Civalleri, K. Doll, N. M. Harrison, I. J. Bush, Ph. D'Arco, and M. Llunell, CRYSTAL09 User's Manual (University of Torino, Torino, 2009).
[25] M. Catti, G. Vallerio, and R. Dovesi, Phys. Rev. B **51**, 7441 (1995).
[26] F. Pascale, C. M. Zicovich-Wilson, F. Lopez Gejo, B. Civalleri, R. Orlando, and R. Dovesi, J. Comput. Chem. **25**, 888 (2004).
[27] W. Stirling, J. Phys.: Sol. St. Phys. **5**, 2711 (1972).

[28]E. Blokhin, E. A. Kotomin, and J. Maier, J. Phys.: Condens. Matter **24**, 104024 (2012).
[29]R. Moos and K. H. Haerdtl, J. Am. Cer. Soc. **80**, 2549 (1997).
[30]V. V. Laguta, M. D. Glinchuk, R. O. Kuzian, S. N. Nokhrin, I. P. Bykov, J. Rosa, L. Jastrabik, and M. G. Karkut, J. Phys.: Condens. Matter **14**, 13813 (2002).
[31]B. Bokstein, M. I. Mendelev, and D. J. Srolovitz, *Thermodynamics and Kinetics in Materials Science: A Short Course* (Oxford University Press, New York, 2005).
[32]R. P. Stoffel, C. Wessel, M. Lumey, and R. Dronkowski, Angew. Chem., Int. Ed. **49**, 5242 (2010).
[33]G. Grimvall, *Thermophysical Properties of Materials* (North-Holland, Amsterdam, 1986).